




Magnesium Green for fluorometric measurement of ATP production does not interfere with mitochondrial respiration

 Luiza HD Cardoso*,  Carolina Doerrier,  Erich Gnaiger

Oroboros Instruments, Innsbruck, Austria

*Corresponding author: luiza.cardoso@orooboros.at

Abstract

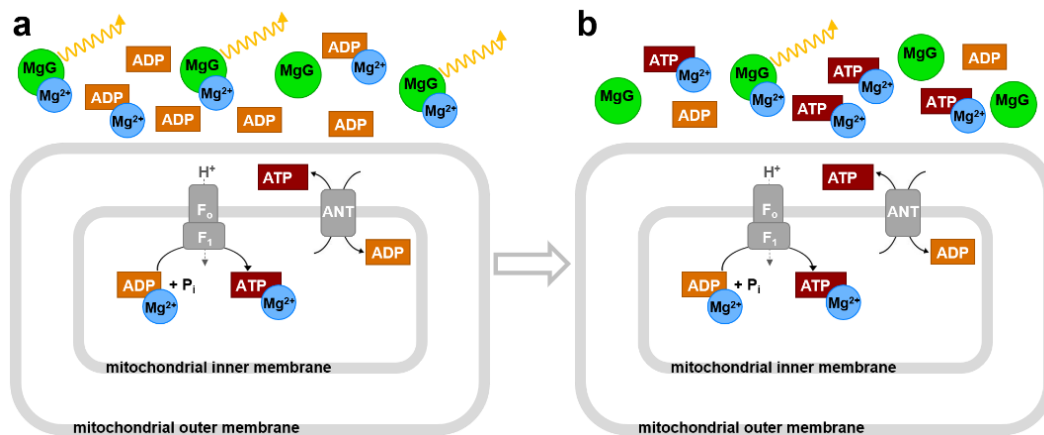
For the advanced study of mitochondrial function, high-resolution respirometry is extended by fluorometric measurement of ATP production using the fluorophore Magnesium Green™ (MgG). A common problem with several fluorescent dyes is the inhibition of mitochondrial respiration. In the present study, a coupling control protocol was applied in combination with MgG to measure ATP production simultaneously with respiration for calculation of $P_{\text{O}_2}/\text{O}_2$ ratios. MgG at 1.1 μM did not affect respiration through the NADH-linked and succinate-linked pathways. Respiration was not inhibited in any of the coupling control states, hence coupling control efficiencies were not affected by MgG.

Keywords – ATP; ATP production; high-resolution respirometry; Magnesium Green; mitochondria; oxidative phosphorylation; fluorometry; FluoRespirometry

1. Introduction

Mitochondrial ATP production can be analyzed with a fluorometric technique using Magnesium Green™ (MgG) as a fluorescent probe, as described by Chinopoulos et al (2009). Application of the Mg^{2+} -sensitive fluorophore as an indicator of ATP production relies on the fact that ADP and ATP have different affinities for Mg^{2+} (Gnaiger, Wyss 1994; Leyssens et al 1996; Budinger et al 1998). ADP is phosphorylated to ATP in the mitochondrial matrix. In the phosphorylation system ADP/ATP and inorganic phosphate P_i are exchanged stoichiometrically by the adenine nucleotide translocase ANT and the phosphate carrier PiC. Under experimental conditions when ADP decreases while ATP increases in the extramitochondrial milieu, the Mg^{2+} concentration declines due to the higher affinity for Mg^{2+} of ATP than ADP (Figure 1). Therefore, the fluorometric assay with the membrane-impermeant MgG provides a quantitative approach to analyze mitochondrial ATP production. This method was developed further to measure concomitantly mitochondrial ATP production and O_2 consumption in the Oroboros O2k-FluoRespirometer which is an experimental system complete for high-resolution respirometry including fluorometry (Chinopoulos et al 2014).

41 Fluorescent dyes are widely used to assess various parameters relevant in
 42 mitochondrial physiology. Safranin, rhodamine and its derivatives, such as TMRM, are
 43 frequently employed as reporters of the mitochondrial membrane potential $\Delta\Psi_p+$.
 44 However, all $\Delta\Psi_p+$ dyes have been shown to affect mitochondrial respiration (Scaduto,
 45 Grotyohann 1999). Like TPP⁺, safranin mainly affects the NADH (N)-linked pathway, the
 46 phosphorylation system, and to a smaller extent the succinate (S)-linked pathway
 47 (Krumshabel et al 2014). The effect of $\Delta\Psi_p+$ fluorescent probes can be explained since
 48 they accumulate in the mitochondrial matrix and thus possibly affect mitochondrial
 49 function.
 50



51 **Figure 1. Concept of the MgG assay according to Chinopoulos et al (2014).** MgG
 52 fluoresces when bound to Mg²⁺. ADP and ATP compete for Mg²⁺ binding with different
 53 affinities; ATP has a higher affinity for Mg²⁺ compared to ADP. **(a)** Initial experimental
 54 conditions, when ADP is added, binding some Mg²⁺, and high MgG fluorescence drops
 55 slightly. **(b)** As the experiment proceeds, ADP is phosphorylated to ATP, which is
 56 exchanged for ADP by the adenine nucleotide translocase ANT. With increase in ATP in
 57 the extramitochondrial medium, more Mg²⁺ is bound to ATP, and MgG fluorescence
 58 decreases.

59
 60 It is important to note that another dye frequently used in mitochondrial physiology
 61 studies, Amplex UltraRed, employed to analyze H₂O₂ production, was shown to affect
 62 mitochondrial respiration even though the mitochondrial membranes are not permeable
 63 to this fluorophore (Makreka-Kuka et al 2015). Therefore, it is important to analyze
 64 whether MgG affects mitochondrial respiration, despite the fact that mitochondrial
 65 membranes are not permeable to this fluorophore.
 66

67 In the present technical communication, we report the effect of MgG on
 68 mitochondrial respiration, which is the gold standard to evaluate mitochondrial function.
 69 This provides an important contribution towards further development of this method to
 70 analyze P_o/O₂ ratios in different mitochondrial preparations. The use of a coupling
 71 control protocol assessing O₂ consumption and MgG fluorescence allows for the
 72 evaluation of mitochondrial respiration and ATP production using NADH- and succinate-
 73 linked substrates in LEAK, OXPHOS- and ET-state, making it possible to obtain flux control
 74 efficiencies.

75 2. Materials and methods

76 2.1. Reagents

77 Magnesium Green was purchased from Invitrogen/Thermo Fisher Scientific (cat. N°
78 M3733). Antimycin A (cat. N° A8674), ATP (cat. N° A2383), CCCP (cat. N° C2759), malate
79 (cat. N° M1000), MgCl₂ 1 M (cat. N° M1028), oligomycin (cat. N° O4876), pyruvate (cat.
80 N° P2256), rotenone (cat. N° R8875), SF 6847 (cat. N° T182), and succinate (cat. N°
81 S2378) were obtained from Sigma Aldrich. ADP was acquired from Millipore (cat. N°
82 117105), and carboxyatractyloside from Calbiochem (cat. N° 216201).
83

84 ADP and ATP were diluted in deionized H₂O without addition of Mg²⁺ salts, pH was
85 adjusted to 6.9 with KOH. Magnesium Green, malate, succinate, carboxyatractyloside and
86 MgCl₂ were diluted in deionized H₂O whereas antimycin A, CCCP, oligomycin, rotenone
87 and SF 6847 were diluted in ethanol p.a. All solutions were aliquoted and stored at -20 °C,
88 except pyruvate, which was diluted in deionized H₂O fresh on the day of each experiment.
89

90 2.2. Animals

91 Wild-type C57BL/6N adult mice (*N*=3 per experimental group) were housed in the
92 animal facility of the Medical University of Innsbruck (maximum 5 mice per cage) and,
93 maintained at 22 °C with a controlled 12 h light/dark cycle. Mice were fed *ad libitum* with
94 free access to water. All procedures were conducted according to the Austrian Animal
95 Experimentation Act in compliance with the European convention for the protection of
96 vertebrate animals used for experimental and other scientific purposes
97 (Tierversuchsgesetz 2012; Directive 2010/63/EU; BMWFM-66.011/0128-
98 WF/V/3b/2016).
99

100 2.3. Cardiac mitochondrial isolation and protein concentration determination

101 Following cervical dislocation, the hearts were immediately excised and transferred
102 into ice-cold biopsy preservation solution (BIOPS: 10 mM Ca²⁺-EGTA - 0.1 μM free Ca²⁺,
103 20 mM imidazole, 20 mM taurine, 50 mM K⁺-MES, 0.5 mM dithiothreitol, 6.56 mM MgCl₂,
104 5.77 mM ATP, 15 mM phosphocreatine, pH 7.1 adjusted with KOH) for short period of
105 time (1–2 h; Fontana-Ayoub et al 2016). All procedures were performed on ice (Gnaiger
106 et al 2000a). Mouse heart mitochondria were isolated following the protocol described
107 by Fontana-Ayoub and Krumschnabel (2015). The heart (~ 80–120 mg) was washed to
108 remove blood clots and minced with 1 mL of BIOPS. The tissue was homogenized with 2
109 mL isolation buffer (IB1: 0.5 M mannitol; 0.5 M sucrose; 0.1 M EGTA; pH 7.4 adjusted with
110 Tris; 2.5 mg/mL BSA and 0.5 mg/mL subtilisin, the latter two added freshly on the day of
111 use) on a 10 mL glass-Teflon Potter Elvehjem homogenizer, 6–8 × with about 1000 rpm
112 mechanical rotation. 3 mL of IB1 was added to the homogenate which was centrifuged at
113 800 *g* for 10 min at 4 °C. The supernatant was centrifuged again, at 10 000 *g* for 10 min at
114 4 °C. The pellet was resuspended carefully using a 1 mL pipette in 0.5 mL IB2 (IB1 without
115 subtilisin). After addition of 2 mL IB2, the homogenate was centrifuged again at 10 000 *g*
116 for 10 min at 4 °C. The pellet was resuspended in 200 μL of IB3 (IB1 without BSA and
117 subtilisin) and kept on ice until use on the same day within 2 h.
118
119
120
121

122 Protein concentration was used for calculation of mass specific O₂ flux, determined
123 using the kit DC Protein Assay (Bio-Rad, Hercules, CA, US). Absorbance was measured at
124 620 nm with a Tecan Infinite TM F200 spectrophotometer (Tecan, Männedorf,
125 Switzerland), using BSA at different concentrations as standards (Lowry et al 1951).

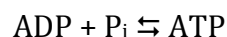
127 *2.4. High-resolution respirometry*

128
129 Oxygen consumption and ATP production measurements were performed
130 simultaneously at 37 °C in the O2k-FluoRespirometer (O2k, Oroboros Instruments,
131 Innsbruck, Austria). The O2k includes two Duran® glass chambers with stirring (750
132 rpm) and controlled temperature for closed-chamber respirometry using polarographic
133 oxygen sensors (POS). Smart Fluo-Sensors Blue were used, with excitation LED 465 nm
134 and filters for the LED and photodiode selected for Magnesium Green™). Specific
135 amperometric emission and detection settings – fluorescence light intensity of 500 and
136 gain 100 – were applied with the software DatLab 7.4 (Oroboros Instruments, Innsbruck,
137 Austria) with continuous data recording set at 2 s time intervals. Standardized
138 calibrations and instrumental O₂ background tests were performed (Doerrier et al 2018).
139 The time-derivative of the O₂ concentration is calculated real-time by DatLab, providing
140 traces of O₂ flux corrected for the O₂ instrumental background (Gnaiger 2001).

141
142 Experiments were run with cardiac isolated mitochondria at protein concentrations
143 in the range of 0.026–0.049 mg/mL in modified mitochondrial respiration medium
144 MiR05-MgG (MgCl₂ 1 mM instead of 3 mM in MiR05, EGTA 0,5 mM, KH₂PO₄ 10 mM, Hepes
145 20 mM, lactobionic acid 60 mM, D-sucrose 110 mM, taurine 20 mM, BSA 1 g/L, pH
146 adjusted with KOH to 7.1). This modification of MiR05 (Gnaiger et al 2000a) was
147 optimized for measurement of ATP production with MgG.

149 *2.5. ATP production measurement with MgG*

150
151 MgG (Magnesium Green™, pentapotassium salt, cell impermeant) does not
152 permeate biological membranes. Therefore, the plasma membrane barrier function must
153 be removed, as achieved in mitochondrial preparations – isolated mitochondria, tissue
154 homogenates, permeabilized tissues and cells. MgG remains outside of the mitochondrial
155 matrix and fluoresces when bound to Mg²⁺. In the phosphorylation reaction



157 reactants and MgG bind Mg²⁺ according to their apparent dissociation constants. When
158 ADP is added to the experimental chamber, there is a fast drop of the fluorescence signal.
159 If mitochondria and fuel substrates are present, ATP is generated and exchanged with
160 ADP by the ANT. ATP has a higher affinity to Mg²⁺ compared to ADP. As ATP concentration
161 increases in the medium, the free Mg²⁺ concentration declines, less MgG is bound to Mg²⁺,
162 and the fluorescence decreases. The ATP concentration in the medium is calculated
163 according to Chinopoulos et al (2009; 2014), taking in account that: (1) the initial
164 concentration of ATP is zero, (2) the initial concentration of ADP is known, (3) the
165 concentration of Mg²⁺ is measured, and (4) apparent *K_d* values for ADP and ATP with Mg²⁺
166 are obtained experimentally.

168 The free Mg^{2+} concentration was calibrated in MiR05-MgG containing the
169 mitochondrial sample, fuel substrates, carboxyatractyloside, and oligomycin. $MgCl_2$ was
170 titrated in 10 steps of 0.1 mM to obtain a non-linear fit for calibration of the amperometric
171 signal. After calibration, the K_d of ADP and ATP for Mg^{2+} was determined for each
172 experimental condition by performing multiple titrations with ADP or ATP.
173

174 2.6. *Substrate-uncoupler-inhibitor-titration (SUIT) protocols*

175

176 Coupling control protocols (SUIT-006) assess different coupling control states -
177 LEAK, OXPHOS and ET - at a constant electron-transfer-pathway state (Gnaiger et al
178 2020). The effect of MgG on mitochondrial respiration was evaluated in its absence or
179 presence (1.1 μM), which was added to the experimental chambers prior to sample
180 addition. Since this fluorescent dye is diluted in water, and only a 2 μL volume was added
181 into the 2 mL chamber, no solvent addition was performed in the control group without
182 MgG. After addition of isolated mitochondria into the O2k chambers, residual oxygen
183 consumption Rox was measured in the absence of substrates. Two coupling-control
184 protocols were used to study simultaneously oxygen consumption and ATP production
185 with the following titrations: NADH-pathway with 5 mM pyruvate and 2 mM malate, or
186 Succinate-pathway with 0.5 μM rotenone and 10 mM succinate. First, LEAK respiration
187 was measured in the absence of ADP. Secondly, OXPHOS capacity was measured after
188 addition of 2 mM ADP. Oligomycin (7.5–10.0 nM) or carboxyatractyloside (0.3 – 0.4 mM)
189 were added to induce again a LEAK state. This was followed by stepwise titration of the
190 uncouplers CCCP (0.5 μM steps) or SF 6847 (25–50 nM steps) up to the optimum
191 concentration, when the maximum O_2 flux was achieved as a measure of ET capacity.
192 Finally, residual oxygen consumption was measured after the addition of the CIII inhibitor
193 antimycin A (2.5 μM).
194

195 2.7. *Data analysis*

196

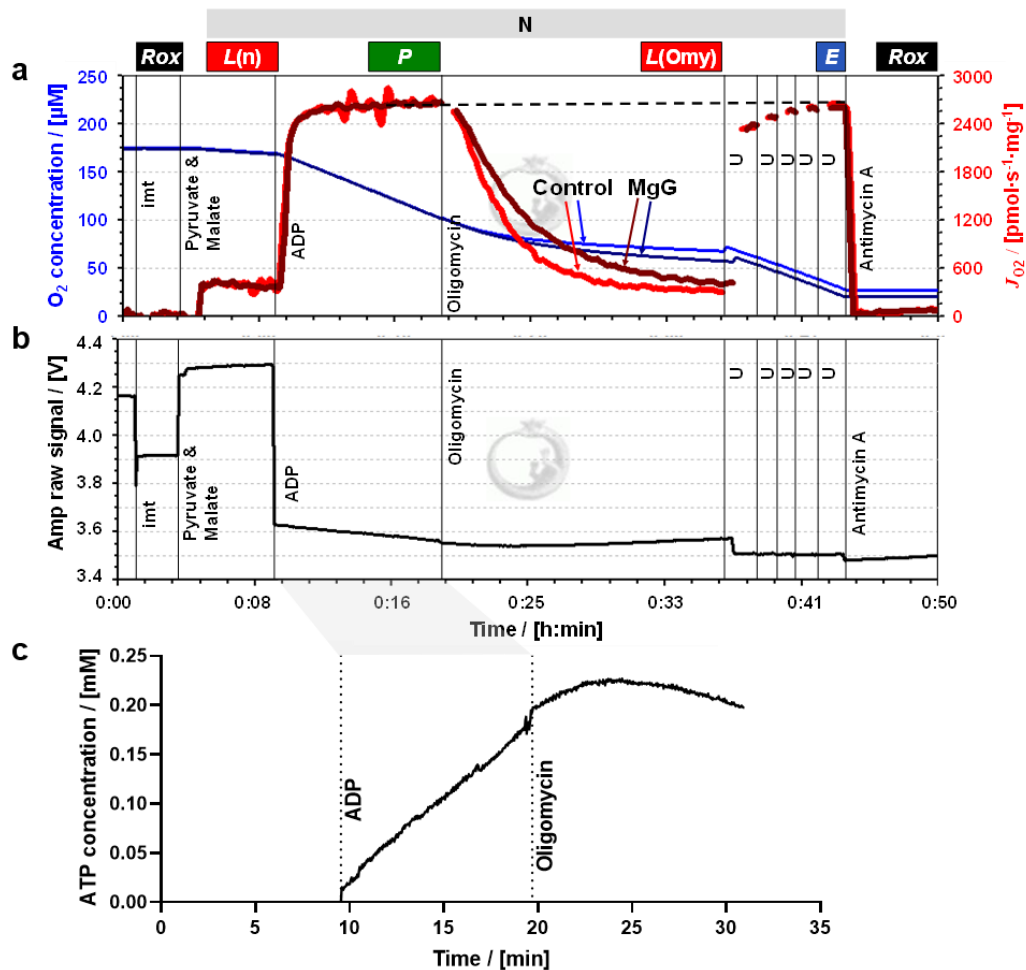
197 The assays were repeated 3 times with independent mitochondrial preparations,
198 with or without MgG, for each condition tested. Data analysis for O_2 consumption,
199 calculations of K_d values and ATP production following Chinopoulos et al 2014, were
200 performed using the templates provided with the software DatLab 7.4.
201

202 3. Results and discussion

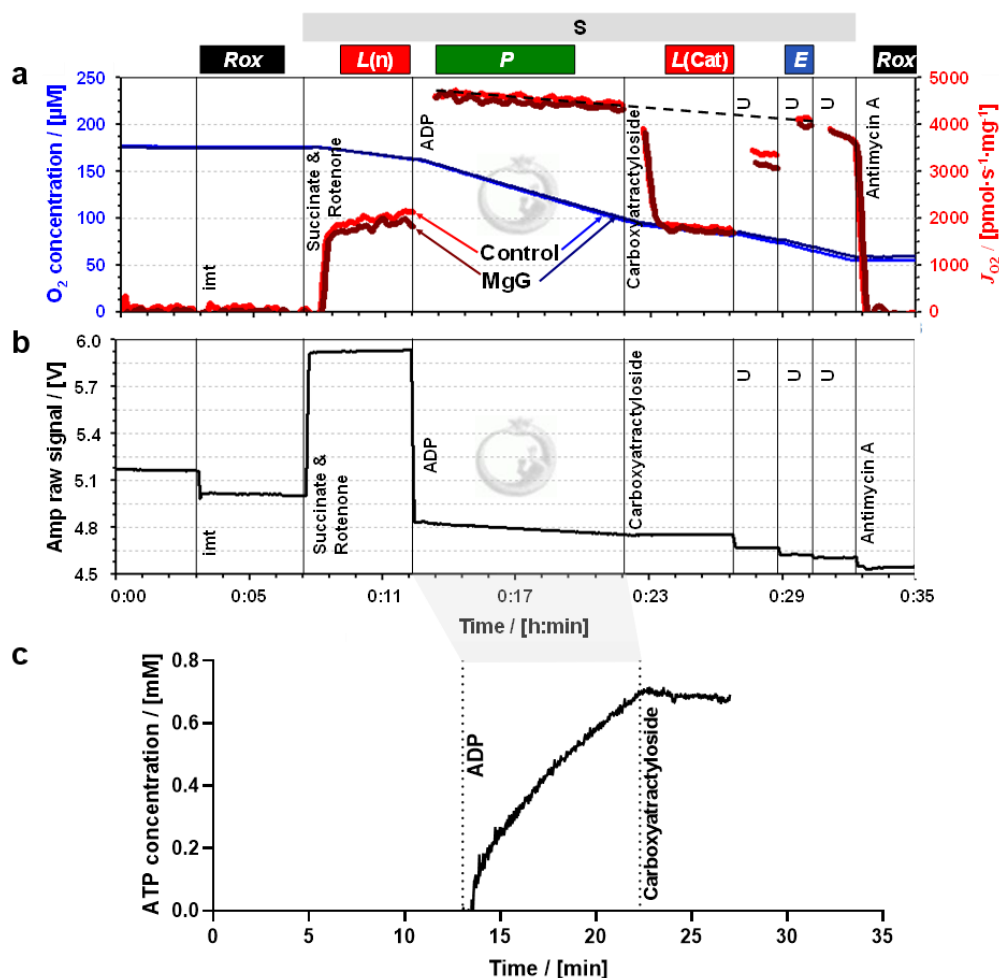
203

204 Figures 2a and 3a show superimposed traces of O_2 concentration and O_2 flux per
205 mass. Coupling control of mitochondrial respiration was measured in two different
206 electron-transfer-pathway control states. In the N-protocol, the NADH-linked pathway
207 through Complex I (CI) was evaluated in the presence of pyruvate and malate which
208 stimulate dehydrogenases of the TCA cycle, leading to reduction of NAD^+ to NADH. NADH
209 is the substrate of CI, with further electron flow into the Q-junction, CIII and CIV (Figure
210 2). In the S-protocol, CI was inhibited by rotenone to prevent reverse electron transfer
211 and accumulation of oxaloacetate, which is an inhibitor of succinate dehydrogenase
212 (Makrecka-Kuka et al 2015; Gnaiger 2020), and respiration was measured supported by
213 succinate as the substrate of CII (Figure 3).

214 In both protocols, LEAK respiration was measured (1) $L(n)$, in the absence of
 215 adenylates and (2) $L(Omy)$ or $L(Cat)$, in the presence of phosphorylation system
 216 inhibitors. Respiration in these two LEAK states was similar, but slightly lower in $L(Omy)$
 217 with the N-protocol (Figure 2a, Table 1). $L(n)$ stabilized quickly, whereas for $L(Omy)$ it
 218 took a long time to fully inhibit respiration by the low concentration of 7.5–10.0 nM
 219 oligomycin. In the S-protocol with sequential addition of rotenone followed by succinate,
 220 $L(n)$ increased for a few minutes until stabilization (Figure 3a). Inhibition by
 221 carboxyatractyloside (0.3–0.4 μM) was immediate, and $L(Cat)$ tended to be slightly lower
 222 than $L(n)$ (Table 1).
 223



224 **Figure 2. Simultaneous measurement of respiration and ATP production by high-**
 225 **resolution Fluorespirometry in mitochondria isolated from mouse heart.**
 226 Representative traces for coupling control protocol SUIT-006 with NADH-linked
 227 substrates (N-protocol), following additions (respiratory states): isolated mitochondria
 228 imt (ROX), pyruvate & malate (LEAK), ADP (OXPHOS), oligomycin (LEAK), uncoupler U
 229 (ET), and antimycin A (ROX). Experiment 2019-02-07 P5 04: **(a)** O_2 concentration (dark
 230 and lighter blue traces) and O_2 flux per mass (dark and lighter red), 1.1 μM MgG versus
 231 control; **(b)** MgG fluorescence signal; **(c)** ATP concentration calculated from MgG signal
 232 calibrated as Mg^{2+} concentration.
 233



234
 235 **Figure 3. Simultaneous measurement of respiration and ATP production by high-**
 236 **resolution Fluorespirometry in mitochondria isolated from mouse heart.**
 237 Representative traces for coupling control protocol SUIT-006 with succinate as substrate
 238 (S-protocol), following additions (respiratory states): isolated mitochondria imt (ROX),
 239 succinate & rotenone (LEAK), ADP (OXPHOS), carboxyatractyloside (LEAK), uncoupler U
 240 (ET), and antimycin A (ROX). Experiment 2019-03-18 P5-03: (a) O_2 concentration (dark
 241 and lighter blue traces) and O_2 flux per mass (dark and lighter red), 1.1 μM MgG versus
 242 control; (b) MgG fluorescence signal; (c) ATP concentration calculated from MgG signal
 243 calibrated as Mg^{2+} concentration.

244
 245 OXPHOS capacity P was measured in the presence of a kinetically saturating
 246 concentration of ADP. The optimum uncoupler concentrations to measure maximum ET
 247 capacity E were 6.0–7.0 μM CCCP in the N-protocol, and 0.150–0.175 μM SF 6847 in the
 248 S-protocol. In the N-protocol, P was stable over time and identical to E . However, in the
 249 S-protocol, P showed a slight decrease over time. Extrapolating this trend of declining O_2
 250 flux to the point where ET capacity was measured explains why E appears to be lower
 251 than P (dashed trendline, Figure 3a). In both protocols, therefore, $E = P$, indicating that
 252 OXPHOS capacity was not limited by the phosphorylation system. This agrees with results

253 for mouse heart mitochondria on coupling control even in the combined NS-pathway
254 (Lemieux et al 2017). Parallel measurements were performed in the presence and
255 absence of 1.1 μM MgG with the N- and S-protocol. This low concentration of MgG used is
256 sufficiently high for calculating ATP production (Figures 2b and c and Figures 3b and c).
257

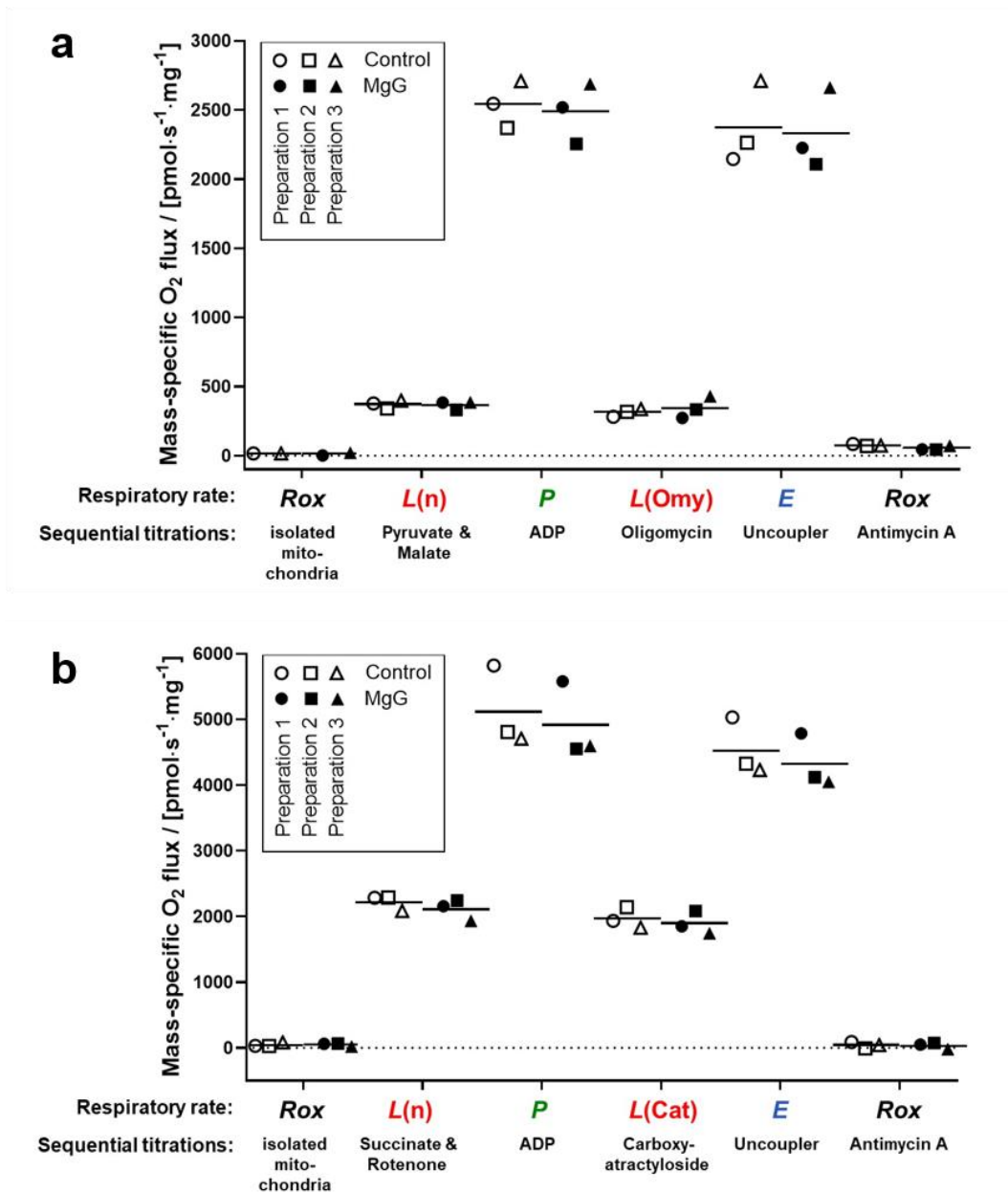
258 The MgG assay to measure ATP production can be used concomitantly with high-
259 resolution respirometry, providing information real-time. Other methods are available to
260 detect ATP production real-time. Spectrophotometric detection of NADPH can be used in
261 conjunction with the coupled enzyme system hexokinase and glucose-6-phosphate
262 dehydrogenase (Horgan, 1978). This assay has been adapted for simultaneous detection
263 of O_2 consumption and NADPH (Lark et al 2016). The luciferin/luciferase assay can be
264 used for continuous measurement of ATP production (Manfredi et al 2002). It is
265 important to note that luciferase consumes O_2 , and instruments typically used for
266 luminometry do not allow monitoring of O_2 concentration in parallel.
267

268 Another method for continuous measurement of the $\text{P}\gg/\text{O}_2$ ratio is the steady-state
269 ADP injection-respirometry (Gnaiger et al 2000b; 2001). The phosphorylation rate is set
270 by continuous injection of ADP as the rate-limiting step while measuring O_2 consumption
271 stimulated to a constant sub-maximal level. Chance and Williams (1955) originally
272 described a polarographic ADP pulse-titration method to determine the $\text{P}\gg/\text{O}_2$ ratio,
273 titrating a known concentration of ADP, which leads to a peak of O_2 consumption
274 stimulated by the complete phosphorylation of ADP to ATP. The ADP pulse-titration
275 method has been extended and critically discussed by Gnaiger (2001).
276

277 End-point assays are available to detect ATP levels, providing discontinuous
278 measurement of ATP production. These include chromatography (high performance
279 liquid chromatography, HPLC; thin layer chromatography, TLC); nuclear magnetic
280 resonance detection of 2-deoxyglucose and its phosphorylated form, and radioactivity
281 measurements using ^{32}P (Menegollo et al 2019; Morciano et al 2017; Fink et al 2017;
282 Sausen et al 2019).
283

284 The fluorometric MgG assay applied simultaneously with O_2 consumption by HRR
285 has been used extensively (Iftikar, Hickey 2013; Goo et al 2013; Chinopoulos et al 2014;
286 Pham et al 2014; Power et al 2014; Salin et al 2016; Napa et al 2017; Masson et al 2017;
287 Salin et al 2018; Devaux et al 2019; Salin et al 2019). Understanding whether MgG may
288 affect respiration is crucial for such studies, particularly for $\text{P}\gg/\text{O}_2$ ratios obtained in
289 different electron-transfer-pathway states.
290

291 It is well established that different dyes commonly applied to measure
292 mitochondrial membrane potential inhibit OXPHOS capacity, *e.g.*, safranin, rhodamine
293 123 and its derivatives TMRM and TMRE (Krumshnabel et al 2014; Scaduto, Grotyohann
294 1999). Surprisingly, Amplex UltraRed used to detect H_2O_2 flux impairs respiration despite
295 not accumulating in the mitochondria (Makrecka-Kuka et al 2015). Therefore, we studied
296 the effect of MgG on respiration. MgG at 1.1 μM did not affect NADH-linked nor succinate-
297 linked respiration in any coupling control state (LEAK, OXPHOS and ET) measured in
298 mitochondria isolated from mouse hearts (Figure 4). In addition, residual oxygen
299 consumption was not affected by MgG.
300



301
 302 **Figure 4. O₂ consumption in the absence and presence of MgG by mitochondria**
 303 **isolated from mouse heart.** The respiratory rates indicated in the abscissa were
 304 measured by HRR with two coupling control protocols SUIT-006, with the following
 305 respiratory states: ROX, LEAK (in the absence of adenylates), OXPHOS, LEAK (in the
 306 presence of inhibitors), ET, and ROX. Sequential titrations are described for **(a)** N-
 307 protocol (experiments 2019-02-05 P3-04, 2019-02-06 P3-03 and 2019-02-07 P5-04) and
 308 **(b)** S-protocol (experiments 2019-03-13 P6-03, 2019-03-14 P3-03 and 2019-03-18 P5-
 309 03). For both graphs the three symbol shapes show independent mitochondrial
 310 preparations, whereas open and closed symbols compare results in controls and in the
 311 presence of MgG from the same preparation; bars represent the average.
 312

313 **Table 1. Coupling control efficiency $(P-L)/P$ and P_{\gg}/O_2 ratio in absence or presence**
 314 **of MgG.** Average \pm SD, $N=3$. OXPHOS capacity P and LEAK respiration L corrected for
 315 residual oxygen consumption Rox . $L(n)/L(inh)$ ratios: L in the absence of adenylates (n)
 316 over L with an inhibitor (inh) of the phosphorylation system, oligomycin Omy or
 317 carboxyatractyloside Cat for the N- or S-pathway, respectively. $L(inh)$ is used in $(P-L)/P$.

Protocol	$(P-L)/P$	$L(n)/L(inh)$	P_{\gg}/O_2	P_{\gg}/O
N-pathway - MgG	0.90 ± 0.01	1.13 ± 0.05	-	-
N-pathway + MgG	0.88 ± 0.02	1.12 ± 0.04	2.33 ± 1.07	1.16 ± 0.53
S-pathway - MgG	0.62 ± 0.05	1.27 ± 0.16	-	-
S-pathway + MgG	0.61 ± 0.05	1.12 ± 0.26	2.78 ± 0.74	1.39 ± 0.37

318
 319 The NADH-pathway has three coupling sites, CI, CIII and CIV, whereas the succinate-
 320 pathway has only the latter two, resulting in a lower P_{\gg}/O_2 ratio. When dividing ATP flux,
 321 calculated from the increase in ATP concentration per time, by the simultaneously
 322 measured O_2 flux, then P_{\gg}/O_2 flux ratios ($J_{P_{\gg}}/J_{O_2}$) are obtained. The P_{\gg}/O_2 is twice the
 323 classical P_{\gg}/O (Table 1). P_{\gg}/O_2 obtained for S-pathway was close to the theoretically
 324 expected value (Gnaiger et al 2020). The result obtained for N-pathway was lower than
 325 expected. A limitation of the present study is the low number of replicates ($N = 3$), with a
 326 high variability of P_{\gg}/O_2 ratios. Further experiments are in preparation.

327
 328 Coupling control efficiencies are closely related to P_{\gg}/O_2 ratios. The coupling
 329 control efficiency is defined as $(E-L)/E$, ranging from 0, at zero coupling, to 1 in a fully
 330 coupled system. In the present case of $P = E$, the coupling control efficiency is expressed
 331 as the $P-L$ control efficiency, $(P-L)/P$ (Gnaiger 2020). As expected, a higher $P-L$ control
 332 efficiency of 0.89 ± 0.02 was found for the N-pathway than 0.62 ± 0.05 for the S-pathway
 333 (pooled data with and without MgG, average \pm standard deviation, $N = 6$; Table 1). These
 334 correspond to a RCR = P/L of 9.6 ± 1.8 for the N-pathway and 2.6 ± 0.3 for the S-pathway.

335
 336 In summary, MgG did not affect respiration in any of the coupling control states.
 337 These results demonstrate that measurement of O_2 consumption is reliable concomitant
 338 with the MgG assay in SUIT protocols with different pathway states and coupling states.
 339

340 Acknowledgements

341 We thank Marco Di Marcello and Manuela Passrigger for expert technical support on media and
 342 chemicals preparation, equipment maintenance and mitochondria isolation. This work was
 343 partially funded by the European Union's Horizon 2020 research and innovation programme
 344 under grant agreement No. 859770, NextGen-O2k project. Contribution to COST Action CA15203
 345 MitoEAGLE.
 346

347 Author contributions

348 LHDC, CD and EG designed the work; LHDC collected and analyzed data and drafted the article;
 349 CD and EG critically revised the article, all authors approved the final version of the manuscript.
 350

351 Conflicts of interest

352 EG is founder and CEO of Oroboros Instruments, Innsbruck, Austria.
 353

354 Data availability

355 Original files are available Open Access at Zenodo repository: [10.5281/zenodo.4032674](https://zenodo.org/record/4032674).

356 Abbreviations

357 Amp amperometric; ANT adenosine nucleotide translocase; BSA bovine serum albumin; CI to CIV
 358 Complex I to IV; CCCP carbonyl cyanide m-chlorophenyl hydrazone; $\Delta\Psi_p+$ mt-membrane
 359 potential; EGTA ethylene glycol tetraacetic acid; *E* ET capacity; ETS electron transfer system; F_0F_1
 360 ATP synthase; Hepes *N*-(2-hydroxyethyl)piperazine-*N'*-(2-ethanesulfonic acid); HRR high-
 361 resolution respirometry; imt isolated mitochondria; J_{O_2} O_2 flux; K_d dissociation constant; *L* LEAK
 362 respiration; LED light-emitting diode; MES 2-(*N*-morpholino)ethanesulfonic acid hydrate; MgG
 363 Magnesium Green; *P* OXPHOS capacity; P_{\gg}/O ADP phosphorylated per atom oxygen consumed;
 364 P_{\gg}/O_2 ADP phosphorylated per molecular oxygen consumed; P_i inorganic phosphate; RCR
 365 respiratory acceptor control ratio; *Rox* residual oxygen consumption; SUIT substrate-uncoupler -
 366 inhibitor-titration; TCA tricarboxylic acid; TMRM tetramethylrhodamine methyl ester; TMRE
 367 tetramethylrhodamine ethyl ester; TPP^+ tetraphenylphosphonium; Tris 2-amino-2-
 368 (hydroxymethyl)-1,3-propanediol; U uncoupler.

370 References

- 371
 372 Budinger GRS, Duranteau J, Chandel NS, Schumacker PT (1998) Hibernation during hypoxia in
 373 cardiomyocytes. Role of mitochondria as the O_2 sensor. *J Biol Chem* 273:3320-6.
 374 Chance B, Williams GR (1955) Respiratory enzymes in oxidative phosphorylation. I. Kinetics of oxygen
 375 utilization. *J Biol Chem* 217:383-93.
 376 Chinopoulos C, Vajda S, Csanady L, Mandi M, Mathe K, Adam-Vizi V (2009) A Novel Kinetic Assay of
 377 Mitochondrial ATP-ADP Exchange Rate Mediated by the ANT. *Biophys J* 96:2490-504.
 378 Chinopoulos C, Kiss G, Kawamata H, Starkov AA (2014) Measurement of ADP-ATP exchange in relation to
 379 mitochondrial transmembrane potential and oxygen consumption. *Methods Enzymol* 542:333-48.
 380 Devaux JBL, Hedges CP, Birch N, Herbert N, Renshaw GMC, Hickey AJR (2019) Acidosis maintains the
 381 function of brain mitochondria in hypoxia-tolerant triplefin fish: a strategy to survive acute hypoxic
 382 exposure? *Front Physiol* 9:1941.
 383 Doerrier C, Garcia-Souza LF, Krumschnabel G, Wohlfarter Y, Mészáros AT, Gnaiger E (2018) High-
 384 Resolution FluoRespirometry and OXPHOS protocols for human cells, permeabilized fibers from small
 385 biopsies of muscle, and isolated mitochondria. *Methods Mol Biol* 1782:31-70.
 386 Fink BD, Bai F, Yu L, Sivitz WI (2017) Regulation of ATP production: dependence on calcium concentration
 387 and respiratory state. *Am J Physiol Cell Physiol* 313:C146-53.
 388 Fontana M, Krumschnabel G (2015) Isolation of mouse heart mitochondria. *Mitochondr Physiol Network*
 389 20.06(01):1-2.
 390 Fontana-Ayoub M, Fasching M, Gnaiger E (2016) Selected media and chemicals for respirometry with
 391 mitochondrial preparations. *Mitochondr Physiol Network* 03.02(18):1-10.
 392 Gnaiger E, Wyss M (1994) Chemical forces in the cell: Calculation for the ATP system. In: *What is Controlling*
 393 *Life?* (Gnaiger E, Gellerich FN, Wyss M, eds) *Modern Trends in BioThermoKinetics* 3. Innsbruck Univ
 394 Press:207-12.
 395 Gnaiger E (2001) Bioenergetics at low oxygen: dependence of respiration and phosphorylation on oxygen
 396 and adenosine diphosphate supply. *Respir Physiol* 128:277-97.
 397 Gnaiger E (2020) Mitochondrial pathways and respiratory control. An introduction to OXPHOS analysis. 5th
 398 ed. *Bioenerg Commun* 2020.2: 112 pp. doi:10.26124/bec:2020-0002.
 399 Gnaiger E et al – MitoEAGLE Task Group (2020) Mitochondrial physiology. *Bioenerg Commun* 2020.1.
 400 doi:10.26124/bec:2020-0001.v1.
 401 Gnaiger E, Kuznetsov AV, Schneeberger S, Seiler R, Brandacher G, Steurer W, Margreiter R (2000a)
 402 Mitochondria in the cold. In: *Life in the Cold* (Heldmaier G, Klingenspor M, eds) Springer, Heidelberg,
 403 Berlin, New York:431-42.
 404 Gnaiger E, Méndez G, Hand SC (2000b) High phosphorylation efficiency and depression of uncoupled
 405 respiration in mitochondria under hypoxia. *Proc Natl Acad Sci U S A* 97:11080-5.
 406 Goo S, Pham T, Han JC, Nielsen P, Taberner A, Hickey A, Loiselle D (2013) Multiscale measurement of cardiac
 407 energetics. *Clin Exp Pharmacol Physiol* 40:671-81.

- 408 Horgan DJ (1978) A spectrophotometric assay of ATP synthesized by sarcoplasmic reticulum. *Aust J Biol Sci*
 409 31:21-4.
- 410 Iftikar FI, Hickey AJ (2013) Do mitochondria limit hot fish hearts? Understanding the role of mitochondrial
 411 function with heat stress in *Notolabrus celidotus*. *PLoS One* 8:e64120.
- 412 Krumschnabel G, Eigentler A, Fasching M, Gnaiger E (2014) Use of safranin for the assessment of
 413 mitochondrial membrane potential by high-resolution respirometry and fluorometry. *Methods Enzymol*
 414 542:163-81.
- 415 Lark DS, Torres MJ, Lin CT, Ryan TE, Anderson EJ, Neuffer PD (2016) Direct real-time quantification of
 416 mitochondrial oxidative phosphorylation efficiency in permeabilized skeletal muscle myofibers. *Am J*
 417 *Physiol Cell Physiol* 311:C239-45.
- 418 Lemieux H, Blier PU, Gnaiger E (2017) Remodeling pathway control of mitochondrial respiratory capacity
 419 by temperature in mouse heart: electron flow through the Q-junction in permeabilized fibers. *Sci Rep*
 420 7:2840, DOI:10.1038/s41598-017-02789-8.
- 421 Leysens A, Nowicky AV, Patterson L, Crompton M, Duchon MR (1996) The relationship between
 422 mitochondrial state, ATP hydrolysis, $[Mg^{2+}]_i$ and $[Ca^{2+}]_i$ studied in isolated rat cardiomyocytes. *J Physiol*
 423 496:111-28.
- 424 Lowry OH, Rosebrough NJ, Farr AL, Randall RJ (1951) Protein measurement with the Folin phenol reagent.
 425 *J Biol Chem* 193:265-275.
- 426 Makrecka-Kuka M, Krumschnabel G, Gnaiger E (2015) High-resolution respirometry for simultaneous
 427 measurement of oxygen and hydrogen peroxide fluxes in permeabilized cells, tissue homogenate and
 428 isolated mitochondria. *Biomolecules* 5:1319-38.
- 429 Manfredi G, Yang L, Gajewski CD, Mattiazzi M (2002) Measurements of ATP in mammalian cells. *Methods*
 430 26:317-26.
- 431 Masson SWC, Hedges CP, Devaux JBL, James CS, Hickey AJR (2017) Mitochondrial glycerol 3-phosphate
 432 facilitates bumblebee pre-flight thermogenesis. *Sci Rep* 7:13107.
- 433 Menegollo M, Tessari I, Bubacco L, Szabadkai G (2019) Determination of ATP, ADP, and AMP Levels by
 434 Reversed-Phase High-Performance Liquid Chromatography in Cultured Cells. *Methods Mol Biol*
 435 1925:223-32.
- 436 Morciano G, Sarti AC, Marchi S, Missiroli S, Falzoni S, Raffaghello L, Pistoia V, Giorgi C, Di Virgilio F, Pinton P
 437 (2017) Use of luciferase probes to measure ATP in living cells and animals. *Nat Protoc* 12:1542-62.
- 438 Napa K, Baeder AC, Witt JE, Rayburn ST, Miller MG, Dallon BW, Gibbs JL, Wilcox SH, Winden DR, Smith JH,
 439 Reynolds PR, Bikman BT (2017) LPS from *P. gingivalis* negatively alters gingival cell mitochondrial
 440 bioenergetics. *Int J Dent* 2017:2697210.
- 441 Pham T, Loisel D, Power A, Hickey AJ (2014) Mitochondrial inefficiencies and anoxic ATP hydrolysis
 442 capacities in diabetic rat heart. *Am J Physiol* 307:C499-507.
- 443 Power A, Pearson N, Pham T, Cheung C, Phillips A, Hickey A (2014) Uncoupling of oxidative phosphorylation
 444 and ATP synthase reversal within the hyperthermic heart. *Physiol Rep* pii:e12138.
- 445 Salin K, Villasevil EM, Auer SK, Anderson GJ, Selman C, Metcalfe NB, Chinopoulos C (2016) Simultaneous
 446 measurement of mitochondrial respiration and ATP production in tissue homogenates and calculation
 447 of effective P/O ratios. *Physiol Rep* 10.14814/phy2.13007.
- 448 Salin K, Villasevil EM, Anderson GJ, Selman C, Chinopoulos C, Metcalfe NB (2018) The RCR and ATP/O
 449 indices can give contradictory messages about mitochondrial efficiency. *Integr Comp Biol* 58:486-94.
- 450 Salin K, Villasevil EM, Anderson GJ, Lamarre SG, Melanson CA, McCarthy I, Selman C, Metcalfe NB (2019)
 451 Differences in mitochondrial efficiency explain individual variation in growth performance. *Proc Biol Sci*
 452 286:20191466.
- 453 Sausen CW, Rogers CM, Bochman ML (2019) Thin-Layer Chromatography and Real-Time Coupled Assays
 454 to Measure ATP Hydrolysis. *Methods Mol Biol* 1999:245-253.
- 455 Scaduto RC Jr, Grotyohann LW (1999) Measurement of mitochondrial membrane potential using
 456 fluorescent rhodamine derivatives. *Biophys J* 76:469-77.

457
 458 **Copyright:** © 2021 The authors. This is an Open Access preprint (not peer-reviewed) distributed
 459 under the terms of the Creative Commons Attribution License, which permits unrestricted use,
 460 distribution, and reproduction in any medium, provided the original authors and source are
 461 credited. © remains with the authors, who have granted MitoFit Preprints an Open Access
 462 publication license in perpetuity.

